A study on giant radio pulses

Karuppusamy, R.

CHAPTER 1

Introduction

1.1 Pulsars - what are they?

The science of radio astronomy was born when the radio engineer Karl Guthe Jansky noticed "a steady hiss type static of unknown origin" (Jansky 1932) and it was soon clear that the radio waves orginated from a source outside the Solar system (Jansky 1933). Since then Radio Astronomy has changed our perception of the Universe profoundly. Examples are the discovery of the 3K microwave background which is generally accepted as the observational evidence of the Big Bang theory; the most distant objects called quasars at the edge of the visible universe and receding at a significant fraction of light speed were first discovered at radio wavelengths; unprecedented spatial resolution was possible only at radio wavelengths using a technique known as Global Very Large Baseline Interferometry.

One of the crowning moments in the history of Radio Astronomy was the serendipitous discovery of radio pulsars in 1967 by the then graduate student Jocelyn Bell. Pulsar is an abbreviation for Pulsating Source of Radio as coined by a journalist. As the term suggests, the signal from pulsars is observed as the periodic fluctuation in intensity or brightness of the received radiation at radio frequencies. The original experiment devised by Jocelyn Bell's advisor, Sir Anthony Hewish was to study short time radio intensity variations of quasars caused by interplenatary scintillation. What was initially suspected to be an undesirable radio interference turned out to be a remarkable discovery, heralding the arrival of pulsar science. The arrival of the pulsed signal four minutes earlier every day firmly establised that the source of the radio waves was outside the Solar system. Together with the periodic nature and small

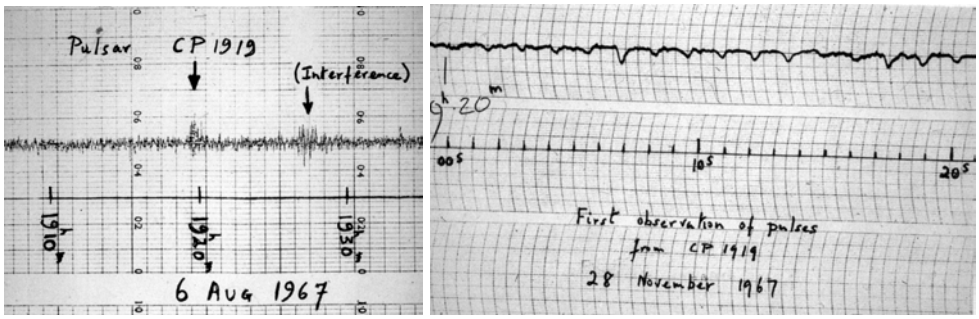

Figure 1.1: (a) A section of paper from Joceyln Bell's chart recorder showing the discovery of PSR B1919+21, originally called CP 1919 (CP stands for Cambridge Pulsar and 1919 its position on the sky in right ascension). (b) A high time resolution measurement showing the individual pulses, seen as dips in the constant baseline with a periodcity of ∼1.34 s.

repetition rates of the signal, it became clear that only a very compact, rotating astronomical body can be the source of the rapidly pulsating radio waves leading to the first experimental evidence for the existence of neutron stars. About three decades earlier, Baade & Zwicky (1934) predicted the possibilty of a neutron star forming when massive stars explode in a supernova. Interestingly, this statement was made only two years after the discovery of the neutron as a chargeless subatomic particle by James Chadwick. In what follows one of the formation scenarios of neutron stars is very briefly reviewed.

1.1.1 Birth of Neutron Stars

Neutron stars are formed during the last stages in the lives of massive stars ($9 - 11\ M_\odot$), when these stars exhaust their fuel reserves and explode as a very bright event called a Type II Supernova. The radiation from a star is powered by the nuclear fusion reactions taking place in the interior of the star. Normally, a star is supported against the gravitational collapse due to its own mass by the radiation pressure from the fusion of lighter atoms to heavier elements which releases energy. However, this "burning" cannot continue indefintely; it ends when Silicon burning terminates with the production of Nickel-56. This is because, beyond this point the formation of any heavier nuclei by means of fusion is an endothermic process; this absorbs energy from the core, thereby altering the temperature and pressure conditions halting the fusion process. This sudden cessation of the radiation pressure from the nuclear burning has a disastrous effect on the star, allowing gravitational forces to takeover. The inevitable gravitational collapse of the star ensues and the result depends on the mass of the stellar core. For core masses between 1.4 to 3 $M_\odot$ the resulting neutron degeneracy pressure halts any further collapse and a neutron star of ∼20 km diameter is born; more massive cores continue to collapse resulting in a black hole. In the case of a neutron star, the original magnetic flux and angular momentum of the star are conserved. Subsequently, the surface magnetic field strength and the rotation speed of the collapsed object are greatly amplified resulting in a highly magnetic, fast spinning neutron star. While the foregoing discussion is

one of the simplest possible formation scenarios, a large magnetic field in the collapsed star can also result from dynamo mechanisms similar to that of the Sun or Earth.

1.1.2 Pulsar Science

The radio emission from the pulsar permits the observation of these objects on the Earth, and is thought to orginate in the region above the magnetic poles of the star. The non-alignment of the rotational and magnetic axis results in a lighthouse-like effect where the "light" is seen only if the rotating beam intersects the Earth. The large magnetic field and rotation result in plasma surrounding the neutron star, and this region is called the magnetosphere. A complete theory of the pulsar radio emission is lacking despite intense study of these objects. It is generally thought that the radio emission is a product of the electron–positron pairs that are accerelated to very high velocities in the magnetosphere of the neutron star. The radio emission from these objects and one particular aspect of the emission is the focus of this thesis.

The large mass, small size and the spin make the neutron stars behave like giant fly-wheels in space. Careful observations of these objects show that the rotation rate decreases with time, implying that the rotation period increases slightly with time. This loss in angular momentum is due to the braking effect from the rotating magnetized neutron star and is termed as magnetic dipole radiation. Therefore, the observed increase in pulse period indicates a loss in the rotational kinetic energy which in turn is equal to the energy radiated away in magnetic dipole radiation. The observed period P and its time derivative $\dot{P}$ of the neutron star can be used to derive some useful quantities. The rotational energy loss is equal to the energy from the magnetic dipole radiation of a rotating magnet with dipole moment $\mathbf{m}$ and can be expressed as,

$$\frac{\mathrm{d}E_{rot}}{\mathrm{d}t} = -\frac{\mathrm{d}(I\Omega^2/2)}{\mathrm{d}t} = \frac{2}{3c^3}|\mathbf{m}|^2\Omega^4 \sin^2\alpha \quad \mathrm{erg\ s^{-1}} \tag{1.1}$$

where $\Omega = 2\pi/P$ is the angular frequency, c is the velocity of light, I is the moment of intertia and α is the angle between the magnetic and rotational axis. The right-hand side of equation 1.1 on rearranging results in an expression that relates $\dot{\Omega}$ and Ω as,

$$\dot{\Omega} = -\left(\frac{2|\mathbf{m}|^2 \sin^2\alpha}{3Ic^3}\right)\Omega^3 \tag{1.2}$$

From the expression above, assuming that the pulsar spindown is entirely due to magnetic dipole radiation, the characteristic age of the pulsar, τ_c is given by,

$$\tau_c = \frac{P}{2\dot{P}} \simeq 15.8\,\mathrm{Myr}\left(\frac{P}{\dot{P}}\right) \tag{1.3}$$

The magnetic field strength at a distance r is $B \approx |\mathbf{m}|/r^3$. Using this and rearranging equation 1.2, the magnetic field strength at the surface of the neutron star in units of Gauss (G) is,

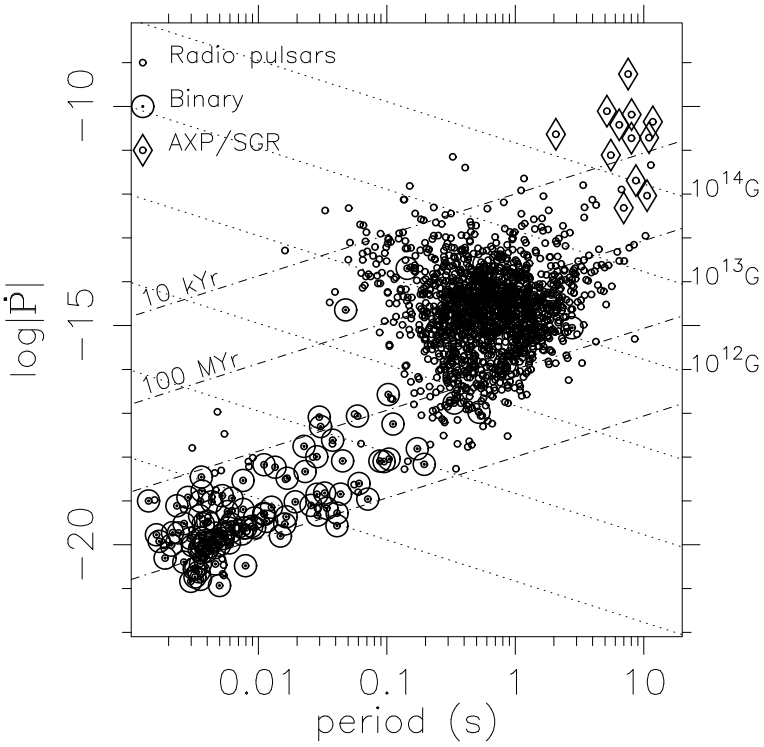

Figure 1.2: The P—$\dot{P}$ diagram showing most known neutron stars. The Anamalous X-Ray Pulsars (AXPs) and Soft Gamma Ray Repeaters (SGRs) are the stars with very large magnetic fields. The symbols shown by dot–circles are binaries, while solitary pulsars are shown by small open circles. The lines of constant characteristic age and surface magnetic field are also shown. This plot was generated using data from the pulsar database maintained by ATNF and is publicly available at http://www.atnf.csiro.au/research/pulsar/psrcat/

$$B_{surf} = \sqrt{\frac{3c^3}{8\pi^2}\frac{I}{R^6 \sin^2\alpha} P\dot{P}} \simeq 10^{12}\mathrm{G}\sqrt{P\dot{P}} \tag{1.4}$$

where R is the stellar radius. The values of P and $\dot{P}$ are plotted for various pulsars in Figure 1.2. Normally a radio pulsar is born with a small pulse period and large magnetic field. As the pulsar evolves, it moves to the lower right part of the $P\dot{P}$ diagram. Some pulsars can be recycled on interaction with another star, and hence be spun up. These pulsars are called millisecond pulsars. They possess comparatively small surface magnetic fields, periods on the order of milliseconds and are found in the lower left corner of the $P\dot{P}$ diagram. The non-interacting or isolated pulsars gradually lose energy and the period increases secularly, eventually becoming radio-quiet objects.

The observed increase in pulse period and the corresponding rate of increase is typically a few nanoseconds per century. Until a few years ago, some pulsars showed rotational accuracies that rivalled the best atomic clocks on the Earth. Only recent developments in atomic timing standards using the so-called fountain atomic clocks offer improved long term stablity [1,2]. The study of the pulsar by means of regular monitoring of the rotation rate is termed as pulsar timing and it holds promise in the first direct detection of gravitational waves, providing one more way to test theories of gravity. Timing observations also permits estimation of the pulsar proper motion and position by transforming the observed arrival times to the solar system barycentre.

At the time of writing this thesis 1826 pulsars are known, with the fastest rotating at 716 times a second (Hessels et al. 2006), and the slowest rotating once in 8.5 seconds (Young et al. 1999). The former is a recycled pulsar, which was spun up to a large rotation rate by the interaction with another star. The latter is a normal middle aged star that will gradually slip into the radio emission graveyard unless spun up by fortutious stellar interaction. Objects like the Crab pulsar studied extensively in this thesis are young objects, with typical spin periods of a few 10's of milliseconds. Many of these young objects are associated with supernova remanents. For example, the Crab pulsar is confirmed to have been produced by a star that exploded in a supernova in 1054 AD.

1.1.3 Pulsar Emission

A simple diagram of a radio pulsar is displayed in Figure 1.3. In the figure, the velocity of light cylinder is the region surrounding the pulsar within which the corotation velocity is less than the speed of light. The radius of this cylinder is also the point where the last open magnetic field line is located and beyond this region the lines open up as the co-rotation breaks.

The rotating radio pulsar can be compared to a giant rotating magnet. This co-rotating magnetic field induces a large electric potential near the surface of the neutron star, several times larger than the gravitational binding potential of the particles to the star. The large potential in turn strips the electrons from stellar surface which begin to stream along the open magnetic field lines. These charged particles in the presence of strong magnetic field results in electron-positron pairs and their motion eventually give rise to the observed radio emission. The radio emission show intensity variations in the range of less then a nanosecond to a several days. The nanosecond variations arise from the temporal plasma inhomogenties while the longer term variations are a result of the changing interstellar medium.

Several models were developed in the past to explain the observed pulsar emission. Currently, a single accepted model does not exist. The main ingredients for pulsar emission to occur are the presence of charged particles and a mechanism to accerelate these particles. One of the first model to be proposed was the force-free electrodynamic (FFE) model, that was initially developed for the aligned rotator (Goldreich & Julian 1969; Komissarov 2002).

[1] The NIST-F1 atomic clock's stability is now measured to be 5×10^{-16} and currently the most accurate. See http://tf.nist.gov/timefreq/cesium/fountain.htm

[2] The PTB's Cesium based fountain atomic clock is stable up to 1×10^{-15}. See http://www.ptb.de/en/wegweiser/infoszurzeit/fragen/04.html

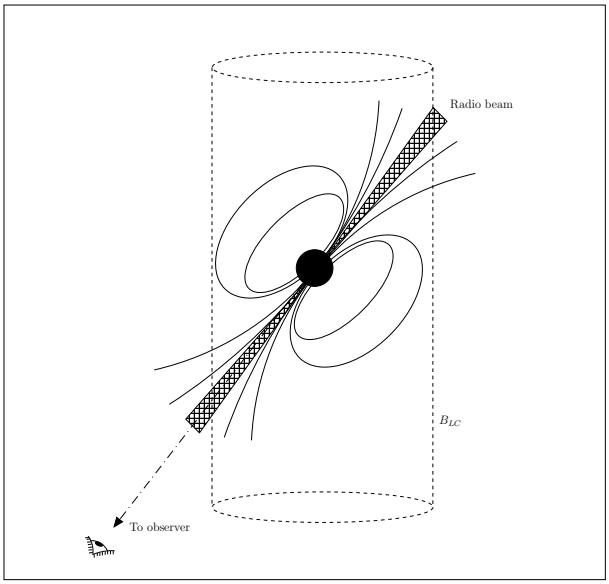

Figure 1.3: A cartoon of the radio pulsar. The velocity of light cylinder is shown, and the magnetic field lines. The radio beam originates above the magnetic poles.

The model is now refined to accommodate the oblique rotator (Spitkovsky 2006) and explains how charged particles, i.e plasma, engulfs a rotating magnetized neutron star. In this model, the rotating magnetic field leads to plasma surrounding the star due to the presence of a large electric field parallel to the stellar surface denoted as $E_{\|}$, and hence extracts charged particles. The motion of these charges occurs either in the slot-gap or the outer magnetosphere gap. The extracted charges are then accerelated along the curved magnetic field lines in these gaps, resulting in curvature radiation (Sturrock 1971; Ruderman & Sutherland 1975). The radio emission in pulsars is usually explained by the slot-gap (Arons & Scharlemann 1979; Muslimov & Harding 2004) and the high energy emission e.g γ-ray emission in the the outer-gap (Cheng et al. 1986; Chiang & Romani 1994) models. In these models, the existence of $E_{\|}$ is predicted. Depending on the model this results in a charge depleted region either in the inner polar cap region, or in the outer magnetosphere, and provides a means to accerelate the charges. Observations with new generation γ-ray telescopes like *Fermi* (Smith et al. 2008; Atwood et al. 2009) can be used to contrain these models.

The signal received by the telescope on Earth as result of the pulsar radio emission is marked by several characteristics. Apart from the first order modulation in the signal's total intensity by the stellar rotation, variations are also observed on a wide range of intensities and timescales. For several applications in pulsar science, e.g pulsar timing, to overcome the weak nature of the single pulses, the average pulse profile is computed and this shows considerable evolution with frequency. While the average pulse profile formed at a given frequency by integrating many individual pulses attains a stable shape with a few hundred to thousand

pulses, the single pulses themselves are rich in features. Some pulsars emit pulses that shows intensity variations within a single pulse period, and are variously called as drifting subpulses, microstructure and giant pulses. Drifting subpulses are features that vary on the order of a few milliseconds; examples are the ordered pulse-to-pulse intensity variation in PSR B0031-07 (Huguenin et al. 1970). Drifting appears to occur in a large fraction of bright pulsars as reported by Weltevrede et al. (2006a). Sensitive analysis methods like the longitude resolved fluctuation spectrum (Backer 1970) and the 2-Dimensional fluction spectrum (Edwards & Stappers 2002) developed in the past allows one to test for the presence of drifting subpulses.

One of the observed features is the increase in the width of the average pulse with the decrease in sky frequency. According to the model above, because of the motion of the charged particles along the magnetic field lines, the radio emission from these particles are tangential to the curved field lines. Moreover, the model also predicts that the number density n of the charged particles vary as r^{-3}, where r is the height above the star. If the observed pulsar radiation is related to the local plasma frequency, then $\nu_p \propto \sqrt{n}$. This gives rise to the so-called radius-to-frequency mapping resulting in lower frequencies emitted higher up in the magnetosphere, where the number density is smaller than the value near the stellar surface. Using multifrequency observations, one can thus determine the emission height of various frequencies.

Intensity variations lasting a few microseconds in some pulsars are quasi-periodic in nature and are called microstructure. In this case, the variations appear to have a characteristic timescale within the single pulse, like the $\sim 570\mu$s structures in PSR B1133+16 (Hankins 1972). Unlike the average emission profile, the microstructure periodicity was found to be independent of the observing frequency prompting some authors to suggest two different emission mechanisms for the pulsed radio emission (Cordes et al. 1990). Various techniques based on autocorrelation analysis have been used to analyse this phenomena, e.g see Lange et al. (1998).

Some pulsars emit extreme pulses in the sense that they last only a few nanoseconds and display extraordinarily large intensities. For example, the giant pulses from the Crab pulsar are known to have an implied brightness temperature of 10^{41}K and can be narrower than 0.4ns (Hankins & Eilek 2007). Similarly, pulses from PSR B1937+21 can be narrower than 15 ns implying brightness temperatures of 10^{37}K (Soglasnov et al. 2004). These narrow pulses can be used as efficient probes of the intervening interstellar medium by studying the observed scatter broadening in these pulses.

The giant pulse emission has also been observed in a few more energetic pulsars but the nature of these pulses is still being debated. Observational evidence points to the prevalence of giant pulse emission in pulsars that have a large value of magnetic field at the velocity of light cylinder, which is denoted as B_{LC} and is related to B_{surf} as follows:

$$B_{LC} = B_{surf}\left(\frac{R}{R_{LC}}\right)^3 \propto P^{-5/2}\dot{P}^{1/2} \tag{1.5}$$

where $R_{LC} = cP/2\pi$ is the light cylinder radius. Currently, a few pulsars with B_{LC} on the order of $\sim 10^5$G show these anamalous emission. Another observational feature is the phase coincidence of the giant pulse emission with the non-thermal high energy emission in some

pulsars. Some models ascribe the giant pulse emission to magnetospheric instablities that give rise to plasma waves (Weatherall 1998). Other models propose Compton scattering of the low frequency radio photons to higher frequencies delivering a large energy in a short time (Petrova 2004). However, a model that accounts for the broad band and coherence on the order of sub-nanosecond timescales of giant pulse emission is not present.

One last feature of the pulsed emission is called nulling and is observed as the complete cessation of the emission that lasts one or more pulse periods. Examples are the nulling phenomena seen in PSRs B1133+16 (Herfindal & Rankin 2007) and B0031-07 (Vivekanand 1995). A form of nulling results in intermittent pulsars, and Kramer et al. (2006) discuss one such example in which the emission toggles between on and off states that can last a few weeks.

1.2 Pulse Dispersion and Scattering

The radio pulsar signal as received by the telescope undergoes two principal propagation effects that smear and broaden the signal as it traverses the ISM. As discussed above, much information on the pulsar emission is contained in the time variation of the pulsed signal and therefore any effect that limits time resolution needs to be corrected. The first is signal dispersion in which the various frequencies emitted by the pulsar travel at slightly different velocities in the ionized interstellar medium. This results in the higher frequencies arriving earlier than the lower frequencies here on Earth. Moreover, the weak nature of the pulsars and the need for high time resolution dictate large bandwidths to improve signal fidelity. However, large observing bandwidths worsen the effect of dispersion smearing, which renders the pulsar undectectable in some cases. Therefore this effect has to corrected for which accurate, high speed hardware is important.

The second propagation effect in the pulsed signal results in pulse scattering and scintillation both of which are due to the multiple paths the signal takes to reach the Earth. The net effect of multi-path propagation in the ISM is the frequency and temporal modulation of the signal from a few minutes to several days over bandwidths of a few KHz to several thousand MHz. Even though this effect cannot be corrected, the effect itself can be used to derive spatial velocities of some pulsars (Cordes 1986).

In what follows, two methods to remove dispersion are reviewed in brief, and more details are found in chapter 2. The pulsed signal can be dedispersed before or after detection. Post-detection dispersion removal involves breaking down the signal using a filter bank to narrow frequency channels, and then adding the signal across the frequency after shifting each filter channel output appropriately. The main aspects of the method is illustrated in Figure 1.4. While this method is relatively straight forward, the smearing in each filter channel remains uncorrected. For many pulsars the dispersion measure, pulse period and sky frequency combinations result in a large smearing even within a frequency channel. Also, the true widths of single narrow pulses cannot be measured using this approach. Therefore, a better method is needed for high time resolution studies.

Pre-detection removal of dispersion is the only way to fully correct pulse smearing and an example is shown in Figure 1.5. The method involves inverting the dispersive effect using

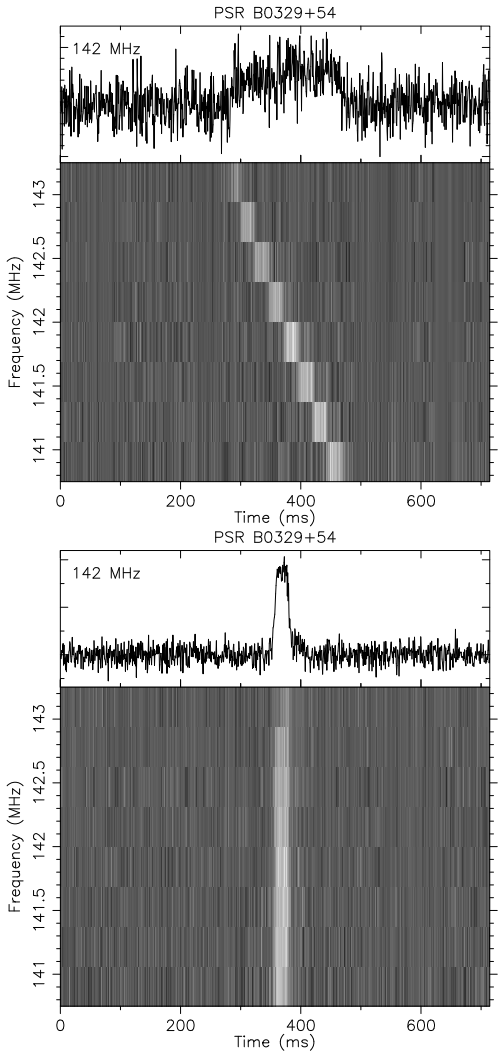

Figure 1.4: Figure showing incoherently dedispersed signal from PSR B0329+54. A 10-second data stretch was folded at the pulse period of 714.51866398 ms and with 8-channel frequency resolution. The top panel shows the dispersion smearing in the signal where lower frequencies arrive later than higher frequencies. The total intensity atop the frequency-phase image shows that the pulse is smeared by $\sim$ 200ms if the dispersion is not removed across the channels. The interchannel delay are shown corrected in the lower panel, but the residual dispersion is still visible within each channel. Note the improved signal fidelity.

a suitable mathematical model of the ISM. The power of this method was recognized and microsecond variations in the pulsed signal of PSR B0950+08 were uncovered in the early

days of pulsar science (Hankins 1971). However, until recently prohibitive computing requirements allowed the application of this technique on either relatively small bandwidths, or on only a few seconds of the pulsar signal.

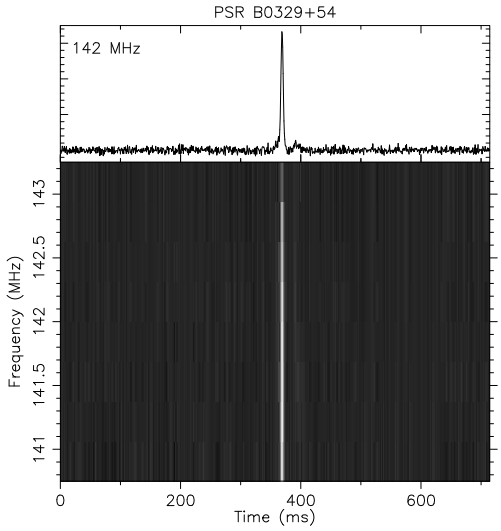

Figure 1.5: Same as in Figure 1.4 but the signal is coherently dedispersed. Both intra- and inter-channel dispersion is removed in this plot. Note the enormous gain in signal-noise-ratio when compared to Figure 1.4.

1.3 Observing pulsars

The pulsar emission gives rise to a propagating electromagnetic wave which ultimately results in the signal received by the radio telescope. This signal is in general very weak. As an illustration, at 1400 MHz sky frequency a pulsar flux density of one Jansky (denoted as Jy) is considered very bright, where 1 Jy = 10^{-26} $\mathrm{Wm^{-2}Hz^{-1}}$. Even with a very sensitive observing system comprising of a radio telescope with 100m parabolic reflector and a detector bandwidth of 20 MHz, this results in a voltage of only 0.3 μV in the antenna probes. This electric potential has to be amplified several million times to detect it.

The minimum detectable signal S_{min} in a radio telescope is the equivalent power measured that corresponds to the smallest increase in the system temperature. Following Lorimer, D. R. and Kramer, M. (2005), this can be expressed as,

$$S_{min} = \frac{T_{sys}}{G\sqrt{N_p \cdot B \cdot T_{int}}} \tag{1.6}$$

where T_{sys} is the system temperature, N_p is the number of polarizations, B is the bandwidth in Hz, T_{int} is the exposure time in seconds, and G is the telescope gain and is equal to $A_e/2k_B$.

k_B is the Boltzmann's constant and A_e is the effective telescope area defined as ηA_p, where A_p is the physical collecting area and effciency factor η is in range 0.1–0.65 depending on the telescope design and frequency of operation.

As evident from equation 1.6 and from the discussion in the previous section, for good sensitivity to the features in pulsar signals one needs a telescope with a large area, a detector with a large bandwidth and low system temperature. High time resolution is also necessary to discern the narrow features in the pulsed signal, which necessitates coherent dedisperion. For these reasons, the pulsed emission from several pulsars in this study were done using the Westerbork Synthesis Radio Telescope (WSRT) and the Pulsar Machine II (PuMa-II). The WSRT is shown in Figure 1.6 and consists of 14 telescopes, each of 25m in diameter. Adding the signals in phase from these telescopes results in the signal equivalent from a telescope of 93m in diameter. Moreover PuMa-II offers coherent dedispersion as a default mode of operation offering a time resolution of up to 50 ns. In addition, the WSRT and PuMa-II combination can offer a bandwidth of 160 MHz resulting in a good sensitivity to narrow and weak pulsed signals.

With the advent of affordable computing, the design and development of the new pulsar machine, PuMa-II is discussed in Chapter 2. The PuMa-II instrument (displayed in Figure. 1.6) was specifically built to coherently dedisperse a large bandwidth (up to 160 MHz) in near realtime allowing pulsar observations up to ~30 hours. The flexibility and high resolution offered by the instrument allows one to study various aspects of pulsars. The operation of PuMa-II results in a large volume of processed data and for this purpose the instrument design also included a 22-TB archive and a 24-tape back up facility capable of accomodating 9.6 TB of storage with a fully loaded magazine.

1.4 Thesis outline

The rest of the thesis is organized as follows: Compared to the previous instrument at the WSRT, PuMa-II improves sensitivity to the pulsar signals by a factor of 4 and provides 50 ns time resolution. This means, a relatively large signal to noise ratio can be acheived in comparatively little time. The combination of high time resolution, full-coherent dedispersion and a large bandwidth provided an excellent oppurtunity to understand some aspects of the enigmatic giant pulse radio emission phenomena, especially from the Crab pulsar. Chapters 3 and 5 present a study of the Crab giant pulses at two sky frequencies. Such a large bandwidth study on a large population of pulses has not been attempted before mainly due to instrument limitations. The giant pulses from the Crab pulsar proved to be sensitive probes of the ISM. Scattering and scintillation were also studied at the two frequencies observed in these chapters.

Within a year of operation of the PuMa-II, the WSRT was equipped with low frequency front ends (LFFEs) that gave access to the skies in the 115–180 MHz radio frequencies. Around this time, it was clear that a very unlikely group of pulsars like B0031-07, B1112+50 and J152+2359 showed giant pulse like emission at low frequencies. In addition, an unrelated experiment at the WSRT showed bright pulses from PSR B1133+16. The emission from these apparently normal pulsars that showed giant pulse like emission predominantly at long

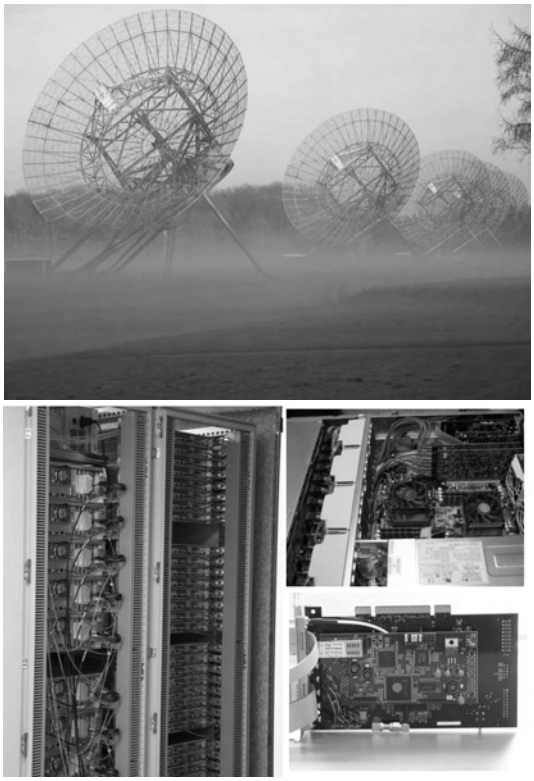

Figure 1.6: A few telescopes of the WSRT are shown in the top panel. Each antenna of the array is parabolic reflector of 25m diameter. Lower panel shows the Pulsar Machine-II (PuMa-II). In the panels on the lower right of the image, one module of PuMa-II is shown with the top cover removed. Custom hardware developed as a part of this thesis work is displayed below this computer module.

radio wavelengths could now be effectively studied with the LFFEs and the PuMa-II. The single pulses collected to examine giant pulse emission also served another purpose – analysis of other pulse features like drifting subpulses and microstructure. This study forms the subject matter of Chapter 4.

The flexible processing in PuMa-II means a single observation can be put through multiple passes of data reduction. This feature was made use for the study of giant pulse emission from millisecond pulsars (MSPs). A few of these pulsars, for example, B1937+21, B1821-24 and J0218+4232 were known to emit giant pulses. Moreover, these pulsars were also routinely observed at the WSRT as a part of the long running pulsar timing programme. The flexibilty of PuMa-II was now put in use to collect more giant pulses from these sources with the aim of better characterisation of the giant pulse emission from the MSPs. Chapter 6 details efforts in this direction. In particular, the efficiency of the piggy-back method to collect additional pulses at nearly no cost is highlighted.

To summarise, the research questions that are being addressed in this work are: Is it possible to design and implement a cost-effective instrument to coherently dedisperse pulsar signals in realtime? Can the time resolution offered by such an instrument provide newer insights in to the narrow giant pulse emission? How does the giant pulse emission change with frequency? Do normal low magnetic field pulsars emit giant pulse? How different are the giant pulse emissions in millisecond pulsars when compared to the Crab giant pulses? Thus this thesis presents results from a research into giant pulse emission from pulsars in different stages of the pulsar life cycle - the young ones like Crab pulsars, followed by older pulsars like B1133+16, B1112+50 and B0031-07, and lastly the very old millisecond pulsars.